PhotoniX

RESEARCH Open Access

An integrated single-shot spectrometer with large bandwidth-resolution ratio and wide operation temperature range

Ang Li[1*], Chang Wang[1], Feixia Bao[1], Wenji Fang[1], Yuxin Liang[2], Rui Cheng[3] and Shilong Pan[1*]

*Correspondence: ang.li@nuaa.edu.cn; pans@nuaa.edu.cn

[1] Key Laboratory of Radar Imaging and Microwave Photonics, Ministry of Education, Nanjing University of Aeronautics and Astronautics, Nanjing 210016, China
[2] United Microelectronics Center, Chongqing 40030, China
[3] School of Instrument Science and Opto-Electronics Engineering, Hefei University of Technology, Hefei, Anhui 230009, China

Abstract

There has been a rapidly growing demand for low-cost, integrated single-shot spectrometers to be embedded in portable intelligent devices. Even though significant progress has been made in this area, two major problems are still remaining, namely the high temperature sensitivity and poor bandwidth-resolution ratio (BRR) that can't meet the requirement of most applications. In this work, we present an integrated single-shot spectrometer relying on a silicon photonic circuit that has a footprint less than 3mm^2, but could achieve broad operation bandwidth about 100 nm and high resolution up to 0.1 nm (with a BRR ~ 1000). Moreover, for the first time, we demonstrate an integrated spectrometer that could operate within a wide temperature range (between 10 and 70 degrees Celsius) without additional power consumption for temperature management.

Keywords: Optical spectrometers, Silicon photonics, Computational spectrometers, Photonic integrated circuits

Introduction

Emerging applications like wearable healthcare devices and portable food scanning equipment are imposing rapidly growing demand for low-cost integrated spectrometers in past decade [1–7]. It is reported that chip-size spectrometers will exhibit a disruptive growth in market value from 2million US dollars in 2019 to over 1.6billion dollars in 2024 [6]. For those applications, single-shot spectrometers are particularly preferred over scanning spectrometers as they do not require additional power consumption and measurement time [7–14]. While to meet the low-cost, Silicon photonics is believed to be one of the most promising platforms to realize integrated single-shot spectrometers-due to its CMOS compatibility that enables wafer-scale fabrication of spectrometers.

Most of the demonstrated single-shot spectrometers on silicon photonics are based on the same principle with free-space based equipment: utilize narrowband optical components such as dispersive gratings or narrowband filters to spatially split the spectral componentsinto different channels (will be described as conventional spectrometers in following context). In other words, each channel produces a

transmission spectrum with non-zero coefficients only within a narrow optical range around certain wavelengthas shown in Fig. 1a, b. Then the measurements from all channels can be simply stitched together to reconstruct the incident spectrum. This technique is straightforward and requires no additional complicated signal processing, thus attracts numerous research attentions [15–21].

But there exist two major limitations for those single-shot spectrometers to be further developed towards commercially available products:

- First is the high temperature sensitivity that requires spectrometers to work at a fixed temperature. Silicon spectrometers based on gratings or narrowband filters typically utilize very long waveguides or resonant cavities to produce narrow transmission bandwidth and high spectral resolution. Consequently, a small amount change in the waveguide refractive index would accumulate and lead to a significant shift in each channel's transmission spectrum [22–24]. Since the channel transmission spectra only contain non-zero components within a narrow optical range, the shift would make the transmissions at certain optical range of interest become zero and the sampling would be lost, which cannot be recovered by any post-processing algorithms. Figure 1c shows simulations results of a simple spectrometer based on an array of 10 silicon ring resonators, supposed to provide spectral sampling between 1541 and 1542.5 nm with a spectral resolution of 0.1 nm. 5 degrees increase in temperature would make the sampling at first 5 channels completely lost. Using integrated heaters can only solve the blue-shift phenomenon induced by decrease in the working temperature, at the cost of additional power consumption. No effective on-chip cooling down approach is demonstrated so far to solve the red-shift problem when working temperature increases.

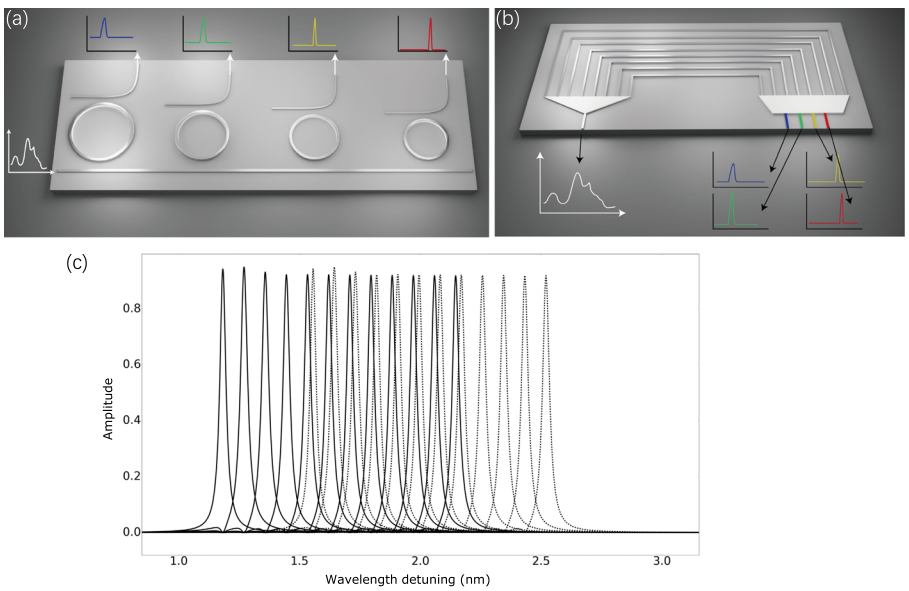

Fig. 1 **a**, **b** Conventional silicon spectrometers using narrowband components such as resonators or dispersive gratings. **c** Temperature change would lead to a significant shift in the narrowband spectrum and for certain optical range of interest, the transmissions will become zero

- Second is the limited bandwidth-resolution ratio (BRR) that can't meet most applications' requirements. bandwidth and resolution are believed to be the most fundamental performance indicators. Large BRR indicates the spectrometer either has broad bandwidth at fixed resolution or high resolution at fixed bandwidth. Therefore, it is a good figure of merit to comprehensively characterize the spectrometers' performance. The BRR of conventional spectrometers. While most applications like Fuel detection, glucose analysis, water pollution, gas analysis would require the spectrometer's BRR over a few hundreds [1]. On the other hand, it is nontrivial for conventional spectrometers to obtain a large BRR, as a series of problems induced by fabrication will be emerging when many grating channels or narrowband filters is present, such as fabrication variations, resonance splitting of resonators, phase errors of gratings etc. Moreover, use many grating channels or narrowband filters would decrease the power received at each detector, leading to poor signal-to-noise ratio and small dynamic range of the spectrometer.

In this work, we propose and validate a computational single-shot spectrometer integrated on silicon photonics platform that successfully overcome the two issues introduced above. It utilizes a novel type of broadband filters called multi-point self-coupled waveguide (MPSCW) to sample the entire spectrum. A single-shot spectrometer consisting of 64 such filters are demonstrated on silicon photonics. The total footprint of the on-chip elements is less than $3mm^2$. The spectrometer's bandwidth exceeds 100nm and the spectral resolution is up to 0.1nm, thus a BRR over 1000 is achieved. Moreover, for the first time, we experimentally demonstrate an integrated spectrometer that can operate within a broad temperature range between 10 and 70 degrees Celsius. Other advantages of this spectrometer included low insertion loss, good scalability and robust to fabrication variations.

Results

Principle of computational spectrometers

Computational spectrometers employ an array of broadband components with non-zero and distinct transmissions within a broad optical range. The schematic of a computational spectrometers and examples of broadband filters spectral responses are plotted in Fig. 2a, b.

The incident signal $\Phi(\lambda)$ will first enter a power splitter to be evenly divided into N portions. Each portion will propagate through a broadband filter with specific spectral response $F_i(\lambda)$, where i = 1,2,3…..N. Consequently, the spectrum at the output of the filter will be modified to $\Phi(\lambda)F_i(\lambda)$, and the response of a photodetector receiving the signal will be the integral of this new spectrum:

$$I_i = R\int_{\lambda_1}^{\lambda_M} \Phi(\lambda)F_i(\lambda)d\lambda \tag{1}$$

where λ_1 and λ_M refer to the starting and ending wavelength of the spectrum, R represents the responsivity of the detector, which is typically wavelength independent and can be pre-calibrated. For signal processing purpose, the integral can be modeled as the product of two discrete arrays:

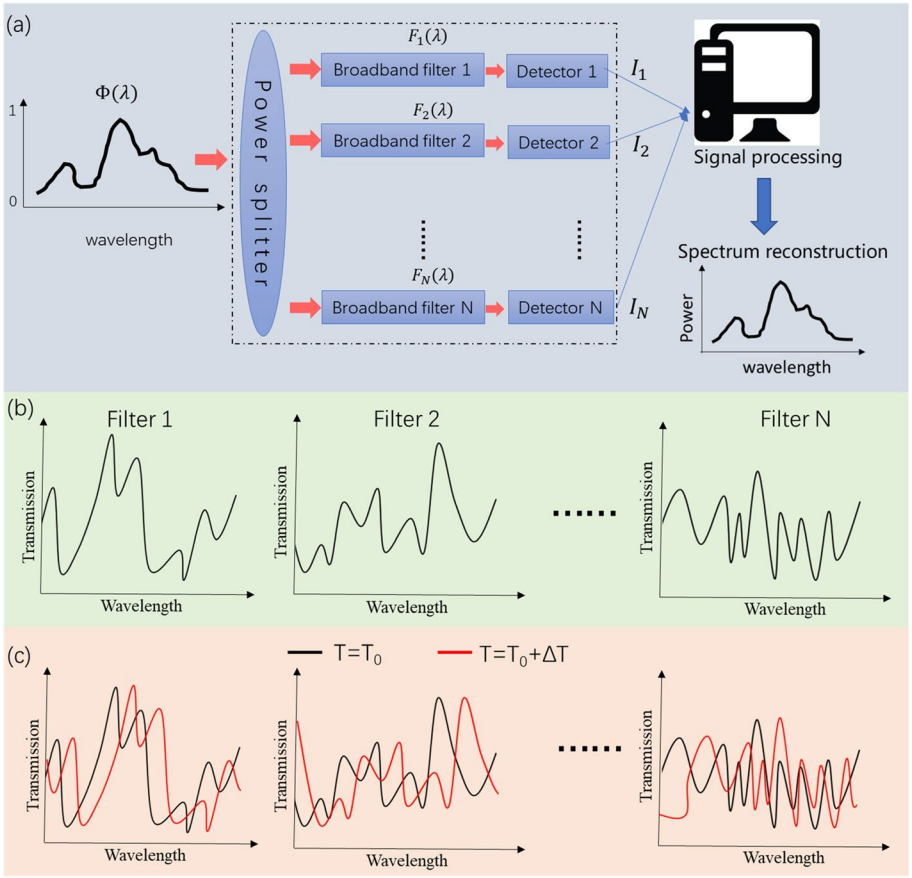

Fig. 2 **a** Schematic of a computational spectrometer that consists of 1xN power splitter and N broadband filters with diverse transmission spectra. **b** Exemplar transmission spectra of broadband filters. **c** Illustration of temperature change induced spectrum shift for broadband filters

$$I_i = R\Phi_{1xM}\Gamma^i_{Mx1} \tag{2}$$

This is a linear equation with M unknowns (Φ_{1xM}), which represent the incident spectrum and M can be considered as the ratio of the bandwidth and resolution of the spectrum. The coefficients of this equation are the transmission coefficients of the filters at corresponding wavelength points and can be obtained at calibration stage. Similarly, N filters with diverse spectral responses (namely, different equation coefficients) will generate N linear equations with M unknowns. For computational spectrometers, the number of equations N can be much smaller than the number of unknowns M, leading to smaller footprint, less splitting loss and larger dynamic range. Under this condition the system becomes under-determined and it should be solved according to Eq. (3) [25, 26]:

$$minimize\ \|I_{1xN} - R\Phi_{1xM}F_{MxN}\|^2 + \alpha\|\Gamma\Phi_{1xM}\|^2\ subject\ to\ 0 \le \Phi \le 1 \tag{3}$$

where I_{1xN} is an array containing responses of N detectors, F_{MxN} is an array whose columns are the filters' spectral responses and α is the regularization coefficient to smooth the results otherwise random spikes will appear due to the nature of the algorithm [25, 26]. Γ is an auxiliary matrix to calculate the derivative of Φ_{1xM}.

Principle to work in a broad temperature range

Temperature change can make the spectrum of any silicon components shift. This problem is unsolvable for conventional spectrometers as discussed in the introduction part andas plotted in Fig. 1c. Therefore, the operation temperature range of conventional silicon spectrometers must be fixed, which seriously limits the development towards commercially available products.

While for computational spectrometers, broadband filters that have non-zero transmissions within a wide optical range are used. The temperature change still shifts the transmission spectrum, but for the optical range of interest, the transmissions are still non-zero and the spectral information would not be lost as shown in Fig. 2c. Mathematically speaking, the spectrometers reconstruct the spectrum by solving Eq. (3), where the sampling matrix F_{MxN} is obtained at calibration stage. F_{MxN} can be considered as a diagonal matrix for conventional spectrometers, and a full matrix for computational spectrometers. When temperature changes, some rows in the F_{MxN} of conventional spectrometers will become zero, leading to spectral info lost of certain wavelengths. But for computational spectrometers, temperature change will only generate a new F_{MxN} and F_{MxN} at different temperatures could be recorded at calibration stage, so that the Eq. (3) can still be solved at different temperatures, simply by choosing correct F_{MxN}. Therefore, employing a simple and cheap temperature sensor is adequate for computational spectrometers to work in a broad temperature range.

Design of novel broadband filters for computational spectrometers

Naturally, the filters spectral responses F_{MxN} would have significant impacts on the quality of solving Eq. (3). For a good computational spectrometer, M and M/N should be large. Large M indicates higher spectral resolution at given bandwidth or broader bandwidth at given spectral resolution. While large M/N means that less filters are required to obtain a given bandwidth/resolution performance. Obviously, for conventional spectrometers, M/N = 1 and M depends on the transmission linewidth of each channel. To obtain large M/N and M simultaneously, the spectral responses of broadband filters should fulfill following requirements:

1. Towards large M, namely high resolution: for computational spectrometers, this can be achieved as long as individual filter's spectral response contains adequate randomness in order to provide high spectral sampling resolution. In other words, it should have more distinguishable responses at two closely separated wavelengths, $|F(\lambda_1) - F(\lambda_1 + \Delta\lambda)| \gg 0$, where $F(\lambda_1)$ refers to the response at λ_1. This can be characterized with the help of auto-correlation of the filter's spectral response.
2. Towards large M/N, namely less filters: Each filter's spectral response needs to be very distinct with others, in other words, the linear dependency between any two filters' spectral responses should be close to zero. Therefore, the sampling of the incident signal using these filters generate independent results. Then a small number of filters is needed to reconstruct unknown spectrum. This can be characterized with the help of cross-correlation of different filters' spectral responses.

To better understand the design guidelines for broadband filters, we provide an illustration of what good and poor spectral responses look like in Fig. 3. Note that the spectral responses are artificially created and should not be related to any physical structures. As shown in Fig. 3a, a good example of filters spectral responses for computational spectrometer should be random and distinct with each other. Its autocorrelation plotted in Fig. 3b shows a main lobe with a Full-Width-Hal-Maximum (FWHM) of 0.5 nm, which can be roughly considered as the spectral sampling resolution. Their cross-correlation is also plotted in Fig. 3b confirming low linear dependency. While Fig. 3c gives a bad example for filters spectral responses, where they are smooth and similar, as evident by the high cross-correlation and broad auto-correlation lobe shown in Fig. 3d. Colloidal quantum dots or Perovskite quantum dots based absorption filters are representatives of smooth and similar spectral responses due to limited design freedom to manipulate (mainly the quantum dots size), thus M/N is only 0.96 and 1.29 respectively [27, 28], and the resolution is limited to above 1 nm. While for spectrometer based on disordered chip or random cavities, the figure of merit M/N becomes much larger due to rich design freedom that can be engineered to tailor the spectral responses [29, 30]. However, they face severe problem of high insertion loss due to additional scattering, radiation and mode mismatch, which seriously degrade their dynamic range and hinder their applications in scenarios that are dealing with weak signals.

This paper proposes and demonstrates a novel type of broadband filters for computational spectrometer that can provide diverse spectral responses with high sampling resolution and exhibit low insertion loss as well as compact footprint. The structure,

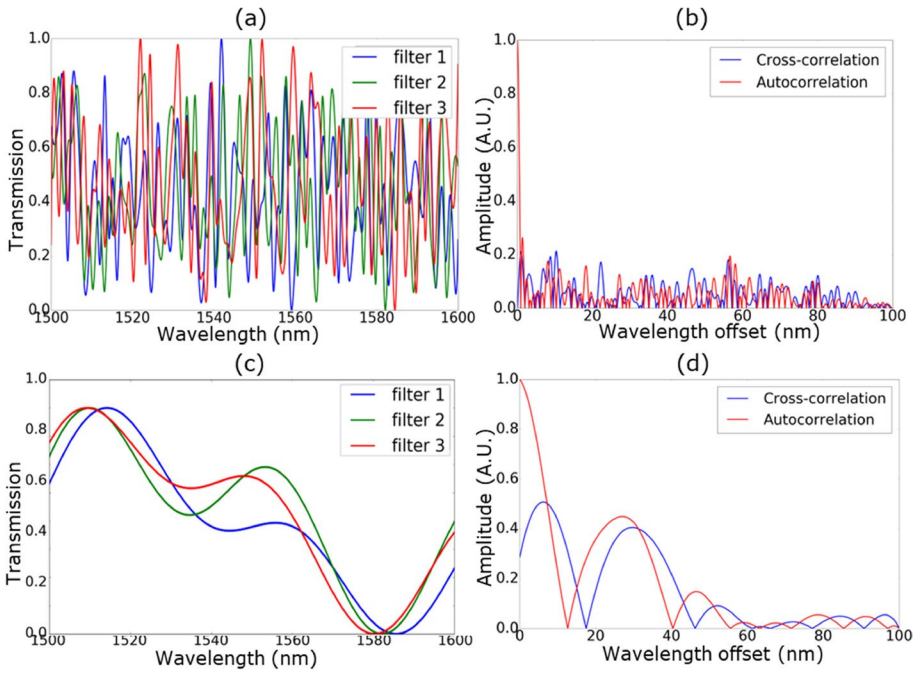

Fig. 3 **a**, **b** show an example of good filters spectral responses for computational spectrometers, the auto- and cross-correlation of the filters' spectral responses, respectively. **c**, **d** show an example of bad filters spectral responses for computational spectrometers, the auto- and cross-correlation of the filters' spectral responses, respectively

called multi-point self-coupling waveguides (MPSCW), is shown in Fig. 4a. The principle is to introduce multiple interference pathways at the output of a waveguide, instead of multiple scattering in those random medium based filters. The interference pathways are induced by multiple evanescent coupling points. The coupling strengths κ of each coupling point and spacings L between any two adjacent couplings can be engineered as design freedom in order to tailor the output spectral response. Therefore, a filter containing 6 coupling points have 11 design freedom (6 coupling coefficients and 5 waveguide lengths), enabling diverse spectral responses. Those 6 coupling points can generate up to 64 potential pathways between input and output, leading to rich interference at the output and consequently high sampling resolution in its spectral responses. Moreover, since it is purely based on waveguide, no additional losses are introduced. We chose silicon photonics as the platform to implement this structure, but it can be transplanted to any other material platform for different optical range of interest, such as Indium Phosphide, Lithium Niobate, Silicon Nitride etc.

We design and simulate 64 filters, each of which has 6 coupling points. All the design freedoms, namely coupling coefficients and spacings between two coupling points, are chosen randomly. But the range for the parameters need to be correctly determined. To understand this, we first set the range for spacings to be (30um, 100um) and vary the value for the coupling coefficients from 0.1 to 0.45 (all couplings are the same). The simulated spectral responses are plotted in Fig. 4b. Clearly, the overall transmission drops when coupling coefficient approaches 0.5. Therefore, to maximize the transmission at the output, the upper limit for the coupling coefficients is set to be 0.1. Then we investigate the impacts of the range for spacings by setting the lower limit of spacing as 30um and varying the upper limit from 35 to 100um. The simulated spectral responses plotted in Fig. 4c suggest increasing the upper limit otherwise the spectral responses will show clear periodicity. The number of coupling points are also studied to understand its

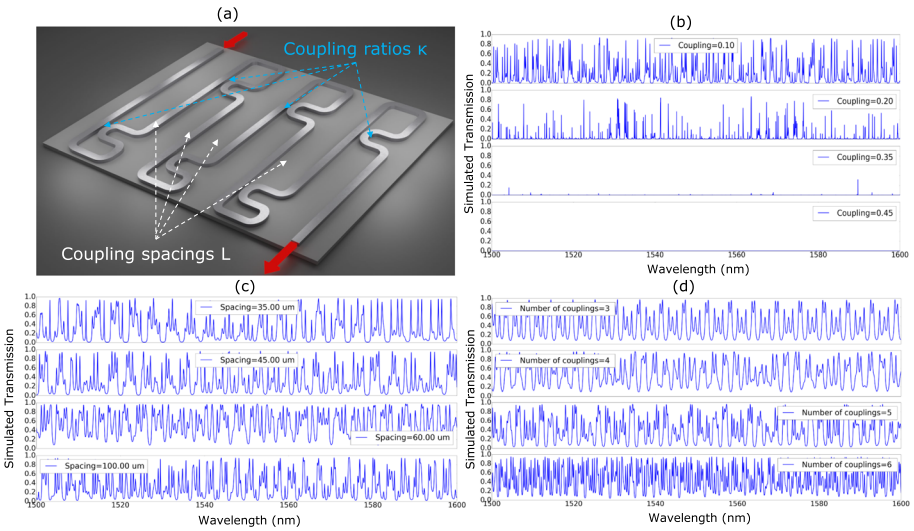

Fig. 4 **a** Schematic of the filter with 4 coupling points. **b** simulated spectral responses with varying coupling coefficients. **c** simulated spectral responses with varying spacing ranges. **d** simulated responses with varying numbers of coupling points

impact on the filter's responses. As shown in Fig. 4d, more coupling points will lead to more random responses, which are ideal for computational spectrometers. Therefore, the filters are designed to have 6 coupling points, and the range for coupling coefficients is (0.01, 01) while the range for spacings is (30um, 100um). Simulated spectral responses of 3 representative filters are plotted in Fig. 5a with an inset providing a zoomed view. Clearly, spectral responses exhibit sharp randomness and are very distinct with each other, as evident by the auto- and cross-correlation shown in Fig. 5b. The FWHM of the main lobe of the auto-correlation is about 0.05 nm, indicating an high sampling resolution. The peak transmissions of those filters are around 0.965 as plotted in Fig. 5(c), suggesting negligible insertion loss. In terms of the power splitter, we use Y-junction tree based structure to ensure small footprint and broad bandwidth. And the Y-junction is designed according to the work presented in [31]. The simulation results confirm its ultra-wide bandwidth, low imbalance between two ports and low insertion loss as evident in Fig. 5d.

Experimental characterization of spectrum reconstruction

The circuit consisting of a 1×64 power splitter based on 5 stage Y-junction tree and 64 broadband filters is fabricated at Applied Nanotools. The fabrication details are introduced in Methods section. The fiber/chip coupling is realized using vertical grating couplers with two-step etch process (70 nm and 220 nm etch depth). Microscopic images of the entire spectrometer and some filters are plotted in Fig. 6a, b, respectively. We first measure the static spectral response of each channel using fiber array. The measurement is performed using a narrow linewidth tunable laser with 1 pm step (Santec TSL710) and a photodetector (Newport). The output from each channel of the fiber array is sent to the photodetector using a 1×64 MEMS optical switch instead of manually connecting and disconnecting. During the measurement, the chip is stabilized on a substrate by

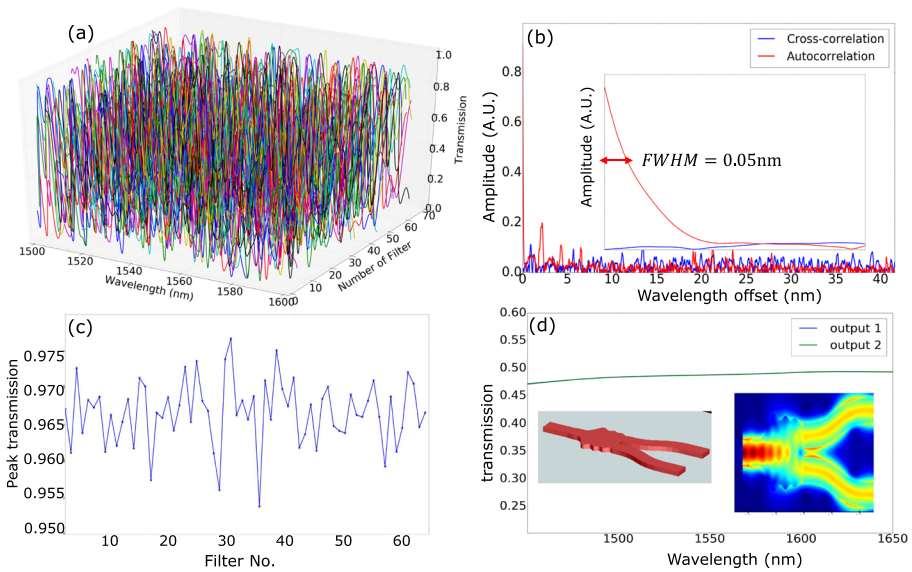

Fig. 5 **a** Simulated spectral responses of the broadband filters; **b** auto- and cross-correlation of the filters' responses; **c** peak transmissions of 64 filters; **d** structure and simulated performance of the Y-junction

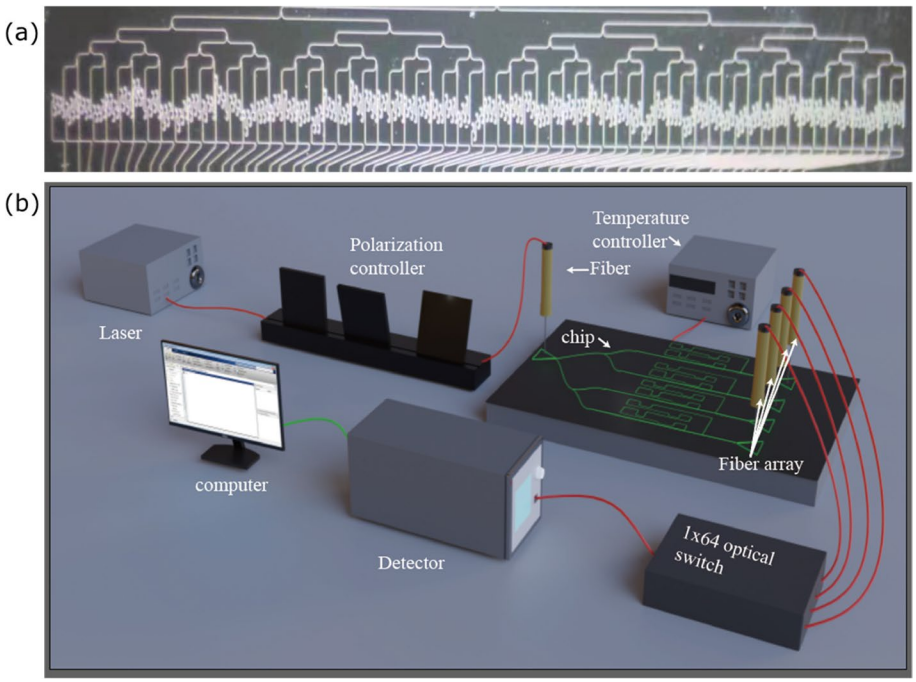

Fig. 6 **a** Microscopic images of the entire spectrometer consisting of 64 filters (**b**) Zoomed view of some filters (**c**) Measurement setup

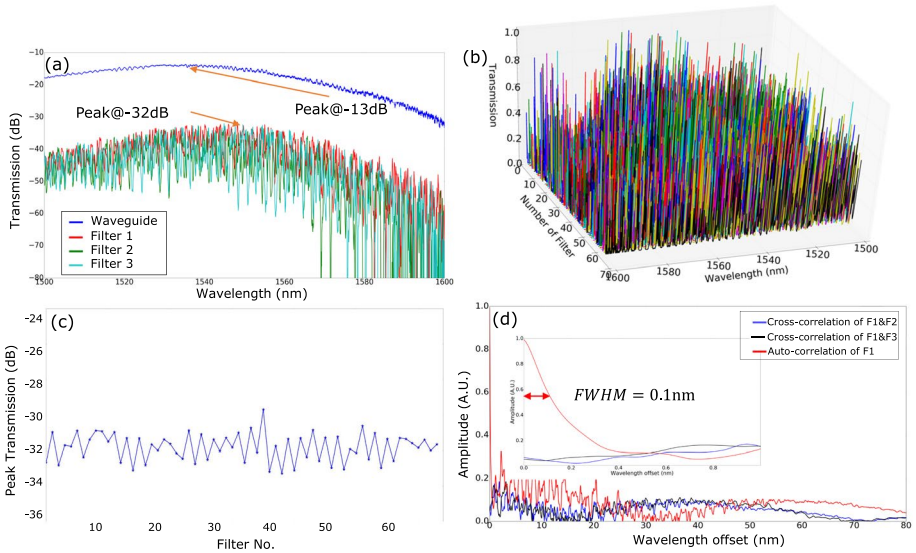

Fig. 7 **a** Spectral responses in log scale of 3 representative channels and a straight waveguide. **b** Spectral responses in linear scale of 64 channels. **c** Peak transmissions of the 64 channels. **d** Auto- and cross-correlations of those spectral responses in (**b**)

vacuum pump to avoid any mechanical vibrations and the temperature is controlled by a temperature controller. The setup is illustrated in Fig. 6c.

Figure 7a, b plot the experimental results of the filters spectral responses in log and linear scale, respectively. The transmission curve of a straight waveguide with two

grating couplers is also given for reference in Fig. 7a. The insertion losses of the filters are first analyzed. It is observed that the peak transmissions of the filters are around -32 dB (ranges from -33 dB till -31 dB, with only one exception higher than -30 dB) as shown in Fig. 7c. The total loss from laser to detector includes setup loss (fiber connectors, polarization controllers etc.), fiber/chip coupling losses and spectrometer's insertion loss (from input to output). The previous two losses amount to about 14 dB according to the transmission curve of a straight waveguide with two grating couplers. Besides, the 1×64 splitter introduces about 18 dB loss to each channel (10*log10(1/64) = -18 dB). Therefore, we could conclude that the insertion loss of the filter itself is negligible, which is in consistency with simulations. The auto- and cross-correlations of some filters' spectral responses are given in Fig. 7d, confirming high sampling resolution around 0.1 nm and very low linear dependency. Note that, the auto-correlation shows certain sidelobes compared with simulations, this is due to the parasitic reflections at the grating couplers that impose a periodic signal on top of the filters' spectral responses. Utilizing low-reflection fiber/chip couplers can effectively reduce this sidelobes [32]. The filter itself is believed to have very broad bandwidth as it is purely based on waveguides, but the fabricated spectrometers have limited bandwidth due to the presence of grating couplers. Using other coupling structures such as edge couplers or subwavelength grating couplers can effectively improve the bandwidth [32].

The spectral responses from each channel are recorded as the matrix RF_{MxN} in Eq. (3). Next, we validate the ability to reconstruct different spectra by sending both broad and narrow spectra to the chip and record the responses from each channel as matrix I_{1xN} in Eq. (3). Then Eq. (3) will be solved using CVX algorithm in MATLAB [33]. We send various spectra to the chip. Those spectra are generated by a broadband halogen light source followed by a Finisar programmable waveshaper with operation range of 1526 nm-1568 nm and minimum resolution of 1 GHz to modify its spectrum. Those spectra are also measured by a commercial Optical Spectrum Analyzer (Anritsu MS9740B, resolution = 0.03 nm) as reference. Before starting the reconstruction of unknow spectra, we need to determine the regularization coefficient in Eq. (3). A spectrum with a 40 nm wide square shape is generated by the waveshaper for calibrating the regularization coefficient as it contains both smooth and sharp spectral features, so that we could better understand the impacts of regularization coefficient. The reconstructions vs various regularization coefficients α are plotted in Fig. 8a. According to the results, larger regularization coefficient would lead to strong distortion, particularly for sharp spectral features, as the regularization is meant to force the spectrum to be smooth. But smaller regularization would result in random spikes on top of smooth spectral components. Therefore, we set the regularization coefficient to be 10^{-5} for reconstructing smooth spectral components and 10^{-6} for narrow spectral components.

Next, another more complicated broadband spectrum containing three broad peaks is sent for reconstruction and the result plotted in Fig. 8b exhibit good accuracy. Figure 8c plots the test results when reconstructing two spectra containing narrowband spectral components. First one is a spectrum with three 0.1 nm wide passbands at 1528 nm, 1545 nm and 1566 nm, respectively. The second spectrum contains three closely standing passbands with around 0.1 nm border-to-border distance. All of

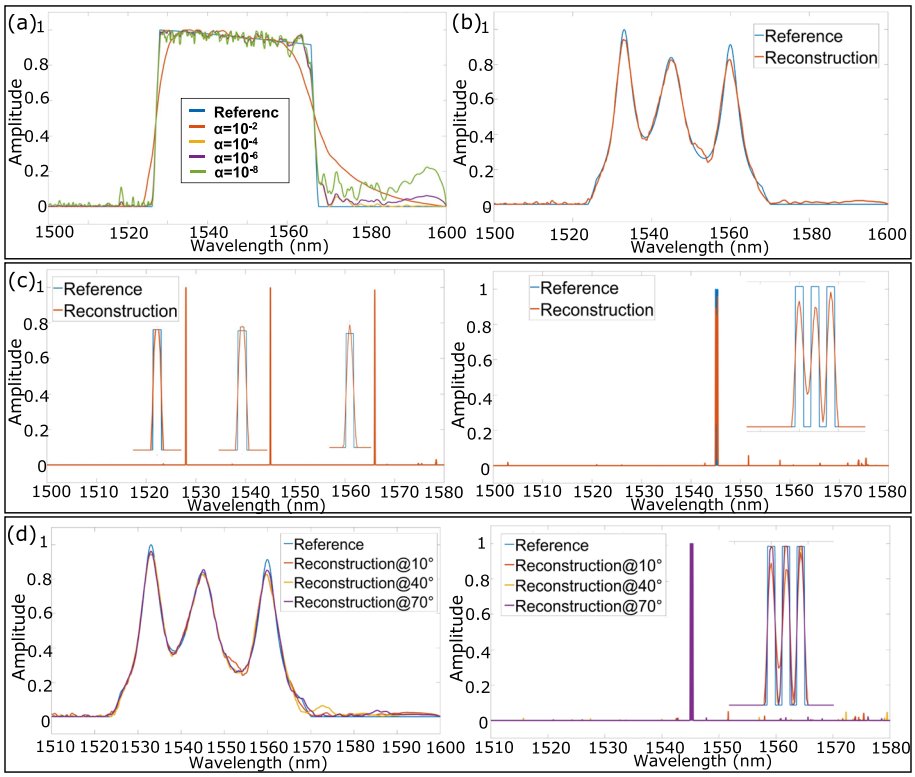

Fig. 8 **a** Reconstruction of a spectrum with a 40 nm wide square shape vs various regularization coefficients. **b** Successful reconstruction of a complicated broadband spectrum. **c** Successful reconstructions of two spectra with narrow components. **d** Successful reconstructions of various spectra under different working temperatures

them can be clearly resolved, which confirms the high resolution of our spectrometer. For all reconstruction procedures, the entire range from 1500 to 1600 nm is digitized to 5,000 points, namely 0.02 nm step size. And those 5,000 unknowns are calculated by solving 64 Eqs. (64 filters). Even if the reconstructed spectra only contain non-zero spectral components within about 50 nm due to equipment limitations, we feel proper to claim the bandwidth and the BRR of our spectrometer to be 100 nm and 1000 respectively, with limitation purely comes from the bandwidths of the grating couplers. The broadband filters' transmission spectra are the only source that limits the bandwidth of the spectrometer and the measured transmission spectra of all filters cover the entire 100 nm range from 1500 to 1600 nm. The cross-correlations within the entire 100 nm range also maintain to a very low level. Therefore, it's safe to expect the spectrometer to operate within this range, as the algorithms or the rest part of the spectrometer are completely wavelength in-dependent.

We also test its ability to work under different temperatures. Besides 10 degrees, each filter's spectral responses at 40 degrees and 70 degrees were also recorded. Then two spectra used in Fig. 8b and c were sent to the spectrometer under 40 degrees and 70 degrees for reconstruction. During the signal processing procedure, the sampling matrix F_{MxN} at corresponding temperatures is chosen to solve Eq. (3). The results plotted in Fig. 8d confirms the spectrometer to work under different temperatures.

This means that for real applications, our spectrometer doesn't require any expensive and power hungry temperature management circuits, instead, a cheap temperature sensor is adequate for our spectrometer to work within a broad temperature range. Note that, the range between 10–70 degrees Celsius should cover the reasonable operating temperature range for practical applications, as this kind of on-chip spectrometers is potentially to be embedded into portable devices such as smartwatches. For temperature beyond this range, particularly for higher temperature, the thermal expansion effect would seriously degrade the coupling conditions between on-chip couplers and free-space mode [8, 11], unless the fiber or other auxiliary coupling elements are permanently attached to the chip. Besides being simple and effective, this method is also universal to any waveguide based computational spectrometers that utilize broadband filters, as long as the transmission spectra of the filters at each temperature are pre-recorded."

To demonstrate a concrete application for integrated spectrometer, we use our spectrometer as together with fiber Bragg grating (FBG) sensor to monitor environmental change. FBG that produce narrowband spectrum can be used as sensors for temperature change, stress change etc. They are extensively used in various applications including fire monitoring, structural healthcare monitoring etc. Typically the environmental change is obtained by analyzing the spectral shift of the FBG. Therefore, a spectrometer is required. We send a broadband source to a FBG (0.1 nm bandwidth centered@1550 nm) and send the reflection to our spectrometer for spectrum reconstruction. The narrowband spectral component can be accurately reconstructed as shown in Fig. 9. Moreover, by applying environmental change such as temperature or stress to the FBG, the spectral shift as small as 0.1 nm can also be clearly resolved as evident in Fig. 9.

Table 1 summarizes recently reported single-shot spectrometers realized on silicon photonics platform, including both conventional spectrometers based on narrowband components and computational spectrometers based on broadband filters. Clearly,

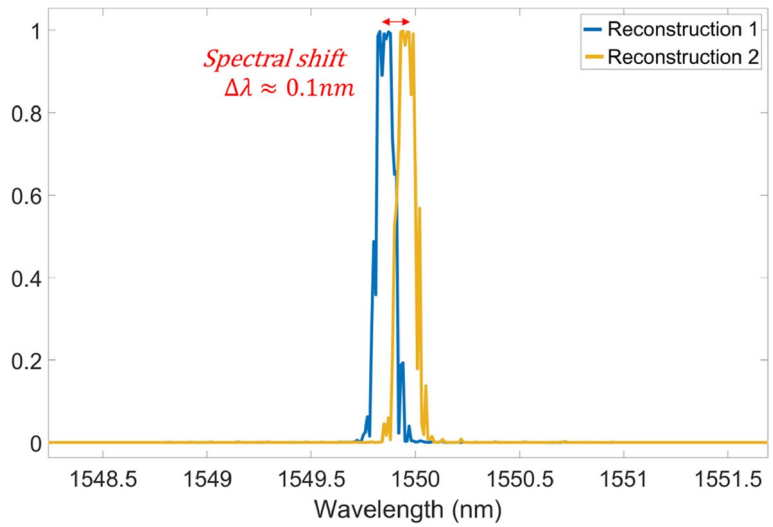

Fig. 9 Using our spectrometer for fiber Bragg grating sensor. A spectral shift caused by either temperature change or stress can be clearly resolved

Table 1 Comparison of various single-shot spectrometers realized on silicon photonics platform

Ref	Spectrometer category	Structure	BRR	Physical channel	Insertion loss
[15]	Conventional spectrometer	Arrayed Waveguide Grating	100	100	Low
[21]		Ring resonators	84	84	Moderate
[20]		Echelle grating	120	121	Low
[29]	Computational spectrometer	Completely disorder chip	33	25	Very high
[34]		Tailored disorder chip	120	8	High
[35]		Spiral multimode waveguide	200	40	Low
[36]		Stratified waveguide filter	400	32	Moderate
Our work		Multi-point self-coupled waveguides	1000	64	Very low

computational spectrometers can achieve a BRR that is much larger than the number of physical channels, which is beneficial in terms of footprint and dynamic range. While among all of the computational spectrometers, our work exhibits impressive advantages of low insertion loss and large BRR. Once again, the BRR of our spectrometer is purely limited by the grating couplers. Using edge couplers could further improve it significantly.

Conclusions

In this paper, we theoretically propose and experimentally demonstrate a computational single-shot spectrometer fully integrated on silicon photonics. The footprint of on-chip components is less than $3mm^2$. It achieves broad operation bandwidth around 100 nm and high resolution of 0.1 nm, thus a BRR over 1000. The bandwidth limitations are mainly from the fiber/chip couplers and the Y-junctions. The broadband filters themselves are believed to have no bandwidth limitations within a few hundred nm. While the resolution can be further improved by incorporating more coupling points to the MPSCW filters. Theoretically, the resolution can be infinitely increased with adequate self-coupling points. But due to the extreme random spectral responses, the minimum number of filters required for spectrum reconstruction would increase. The superior performance is enabled by an array of novel broadband filters, which is called multi-point self-coupling waveguide filters. The filter is based on waveguide structure and introduces negligible additional losses, leading to large dynamic range. It has rich design freedom therefore facilitating diverse spectral responses that exhibit sharp randomness and low linear dependency among different filters. 64 filters are employed for both broadband spectra and narrowband spectra reconstructions. Moreover, for the first time, we experimentally demonstrate an integrated spectrometer to work in a broad temperature range without power-hungry temperature management system. Based on performance requirements of spectrometers for varying applications [1], the broad bandwidth and high resolution of our spectrometer makes it a good candidate for atmospheric monitoring, agricultural and food scanning, lactate and glucose monitoring etc. As it can be fully integrated on a single chip (potentially with photodetector integrated) and requires no additional power consumption for thermal management, it is suitable to be embedded into

power-sensitive portable devices for broader application scenarios. Our work significantly increases the readiness of integrated spectrometers to be used in commercial products.

Methods

The circuit consisting of a 1×64 power splitter based on 5 stage Y-junction tree and 64 broadband filters is fabricated at Applied Nanotools. The structures were defined on a 220 nm thick silicon-on-insulator wafer using E-beam lithography with high fabrication accuracy, with feature size reported to be less than 60 nm. The layout area is about 9mmx9mm, but no noticeable stitching errors are present. The structure layer is sitting on top of a 2um thick buried oxide layer to prevent leakage to the 725um handle wafer and covered by a 3um thick oxide cladding layer for protection. The patterning process begins by cleaning and spin-coating a material that is sensitive to electron beam exposure. A device pattern is defined into this material using 100 keV EBL. Once the material has been chemically developed, an anisotropic ICP-RIE etching process is performed on the substrate to transfer the pattern into the underlying silicon layer. The etch is performed until there is no remaining silicon and the underlying oxide layer is exposed. The fiber/chip coupling is realized by using vertical grating couplers with two-step etch process (70 nm and 220 nm etch depth). The measurement is performed using a narrow linewidth tunable laser with 1 pm step (Santec TSL710) and a commercial photodetector. Fiber array is used to collect light out of the chip. The output from each channel is sent to the photodetector using a 1×64 MEMS optical switch instead of manually connecting and disconnecting. During the measurement, the chip is stabilized on a substrate by vacuum pump and the temperature is controlled by a TEC to avoid any mechanical vibrations and temperature fluctuations.

Abbreviations

BBR	Bandwidth-resolution ratio
CMOS	Complementary Metal–Oxide–Semiconductor
MPSCW	Multi-point self-coupled waveguide
FWHM	Full-Width-Half-Maximum
SNR	Signal-to-noise ratio
MEMS	Micro-electro-mechanical system
TEC	Temperature Controller
FBG	Fiber Bragg grating

Supplementary Information

The online version contains supplementary material available at https://doi.org/10.1186/s43074-023-00109-0.

Additional file 1: Fig. 1. Reconstruction errors as a function of noise strength added to the detector responses. **Fig. 2.** (a-b) detector responses with/without noise and (c-d) the reconstructed results at =0.02 and 0.06.

Authors' contributions

AL conceived the idea. CW, FB and WF designed the layout and participated in simulations and measurements. AL performed most of the simulations and measurements. AL, YL and RC performed the data analysis. SP supervised this work and reviewed the manuscript. All authors read and approved the final manuscript.

Funding

This work is supported by National Key R&D Program of China (grant No. 2021YFB2801500), National Natural Science Foundation of China (grant No. 62105149, No. 62375126), Fundamental Research Funds for the Central Universities (grant No. NS2022043), Provincial Distinguished Professor Fund of Jiangsu, Natural Science Foundation of Jiangsu Province (grant No. BK20210288) and State Key Laboratory of Advanced Optical Communication Systems and Networks, China.

Availability of data and materials
Availability of code, data, and/or materials used in the research results reported in the manuscript may be provided upon reasonable request.

Declarations

Ethical approval and consent to participate
All authors participate in this work and manuscript.

Consent for publication
All authors agree with the submission of this manuscript

Competing interests
The authors declare no conflicts of interest.

Received: 14 March 2023 Revised: 1 September 2023 Accepted: 7 September 2023
Published online: 20 September 2023

References

1. Li A, et al. Advances in cost-effective integrated spectrometers. Light Science Applications. 2022;11(1):174.
2. Bacon CP, Mattley Y, DeFrece R. Miniature spectroscopic instrumentation: Applications to biology and chemistry. Rev Sci Instrum. 2004;75(1):1–16.
3. Yang Z, et al. Miniaturization of optical spectrometers. Science. 2021;371(6528):eabe0722.
4. McGonigle AJ, et al. Smartphone spectrometers. Sensors. 2018;18(1):223.
5. Crocombe RA. Portable spectroscopy. Appl Spectrosc. 2018;72(12):1701–51.
6. Kulakowski, J. and B. d'Humières, Miniature, micro and chip-size spectrometers: technologies, market trends and customers' needs. 2020, Tematys.
7. Zhang J, et al. Cascaded nanobeam spectrometer with high resolution and scalability. Optica. 2022;9(5):517–21.
8. Li A, Fainman Y. Integrated silicon Fourier transform spectrometer with broad bandwidth and ultra-high resolution. Laser & Photonics Reviews. 2021;202000358:200358.
9. Zhang Z, Wang Y, Tsang HK. Tandem configuration of microrings and arrayed waveguide gratings for a high-resolution and broadband stationary optical spectrometer at 860 nm. ACS Photonics. 2021;8(5):1251–7.
10. Pohl D, et al. An integrated broadband spectrometer on thin-film lithium niobate. Nat Photonics. 2020;14(1):24–9.
11. Li A, et al. Fabrication-tolerant Fourier transform spectrometer on silicon with broad bandwidth and high resolution. Photonics Research. 2020;8(2):219–24.
12. Zheng SN, et al. Microring resonator-assisted Fourier transform spectrometer with enhanced resolution and large bandwidth in single chip solution. Nat Commun. 2019;10(1):1–8.
13. Zheng S, et al. A single-chip integrated spectrometer via tunable microring resonator array. IEEE Photonics J. 2019;11(5):1–9.
14. Kita DM, et al. High-performance and scalable on-chip digital Fourier transform spectroscopy. Nat Commun. 2018;9(1):1–7.
15. Cheben P, et al. A high-resolution silicon-on-insulator arrayed waveguide grating microspectrometer with sub-micrometer aperture waveguides. Opt Express. 2007;15(5):2299–306.
16. Ma X, Li M, He J-J. CMOS-compatible integrated spectrometer based on echelle diffraction grating and MSM photodetector array. IEEE Photonics J. 2013;5(2):6600807–6600807.
17. Ryckeboer E, et al. Silicon-on-insulator spectrometers with integrated GaInAsSb photodiodes for wide-band spectroscopy from 1510 to 2300 nm. Opt Express. 2013;21(5):6101–8.
18. Ryckeboer E, et al. CMOS-compatible silicon nitride spectrometers for lab-on-a-chip spectral sensing. in Silicon Photonics and Photonic Integrated Circuits V. 2016. International Society for Optics and Photonics. Proceedings of the SPIE. 2016;9891:9. id. 98911K.
19. Fan T, et al. Highly-uniform resonator-based visible spectrometer on a Si 3 N 4 platform with robust and accurate post-fabrication trimming. Opt Lett. 2018;43(20):4887–90.
20. Ma K, et al. High-resolution compact on-chip spectrometer based on an echelle grating with densely packed waveguide array. IEEE Photonics J. 2018;11(1):1–7.
21. Xia Z, et al. High resolution on-chip spectroscopy based on miniaturized microdonut resonators. Opt Express. 2011;19(13):12356–64.
22. Dong P, et al. Thermally tunable silicon racetrack resonators with ultralow tuning power. Opt Express. 2010;18(19):20298–304.
23. Li A, Bogaerts W. Experimental demonstration of a single silicon ring resonator with an ultra-wide FSR and tuning range. Opt Lett. 2017;42(23):4986–9.
24. Yang Y, et al. Thermo-optically tunable silicon AWG with above 600 GHz channel tunability. IEEE Photonics Technol Lett. 2015;27(22):2351–4.
25. Donoho, D.L., Neighborly polytopes and sparse solutions of underdetermined linear equations. 2005.
26. He F, Gaston KJ. Estimating abundance from occurrence: an underdetermined problem. Am Nat. 2007;170(4):655–9.
27. Bao J, Bawendi MG. A colloidal quantum dot spectrometer. Nature. 2015;523(7558):67–70.
28. Zhu X, et al. Broadband perovskite quantum dot spectrometer beyond human visual resolution. Light Science Applications. 2020;9(1):1–9.
29. Redding B, et al. Compact spectrometer based on a disordered photonic chip. Nat Photonics. 2013;7(9):746–51.

30. Wang Z, et al. Single-shot on-chip spectral sensors based on photonic crystal slabs. Nat Commun. 2019;10(1):1–6.
31. Zhang Y, et al. A compact and low loss Y-junction for submicron silicon waveguide. Opt Express. 2013;21(1):1310–6.
32. Wang Y, et al. Design of broadband subwavelength grating couplers with low back reflection. Opt Lett. 2015;40(20):4647–50.
33. Grant M, Boyd S. CVX: Matlab software for disciplined convex programming, version 2.1. 2014. http://cvxr.com/cvx/citing/.
34. Hadibrata W, et al. Compact, High-resolution Inverse-Designed On-Chip Spectrometer Based on Tailored Disorder Modes. Laser Photonics Rev. 2021;15(9):2000556.
35. Redding B, et al. Evanescently coupled multimode spiral spectrometer. Optica. 2016;3(9):956–62.
36. Li A, Fainman Y. On-chip spectrometers using stratified waveguide filters. Nat Commun. 2021;12(1):2704.

Publisher's Note